Inorganic Chemistry
Article

Inorg. Chem. **2009**, *48*, 8439–8444 **8439**
DOI: 10.1021/ic901043g

Synthesis, Structure, and Magnetic Properties of $Na_3LnMn_3O_3(AsO_4)_3$ (Ln = La, Sm, and Gd): A New 3d-4f Series Exhibiting One-Dimensional Manganese(III) Oxide Chains Connected via LnO_9 Units

J. Palmer West, Shiou-Jyh Hwu,* and Wendy L. Queen

Department of Chemistry, Clemson University, Clemson, South Carolina 29634-0973

Received May 30, 2009

In attempts to synthesize compounds containing mixed lanthanide and transition metal oxide magnetic nanostructures, a new 3d-4f arsenate phase, $Na_3GdMn_3O_3(AsO_4)_3$, was isolated using high-temperature, molten-salt methods. The X-ray single-crystal structure analysis shows that $Na_3GdMn_3O_3(AsO_4)_3$ crystallizes in a hexagonal space group with $a = 11.091(2)$ Å, $c = 5.954(1)$ Å, and $V = 634.2(2)$ Å^3; $P6_3/m$ (No.176); $Z = 2$. The structure has been refined by full-matrix, least-squares methods to a final solution with R1 = 0.0466, wR2 = 0.1318 and GOF = 1.101. This new three-dimensional framework consists of ferromagnetic one-dimensional $[MnO_4]_\infty$ chains, composed of edge-shared MnO_6 units propagating along *c*. The GdO_9 polyhedra connect three neighboring $[MnO_4]_\infty$ chains via oxygen atoms. $Na_3LaMn_3O_3(AsO_4)_3$ (**1**), and $Na_3SmMn_3O_3(AsO_4)_3$ (**2**), the isostructural derivatives of $Na_3GdMn_3O_3(AsO_4)_3$ (**3**), were synthesized to acquire additional insight into the 3d-4f magnetic couplings. The $Na_3LnMn_3O_3(AsO_4)_3$ series reveals an increase in χT at low temperatures upon substitution of smaller Ln^{3+} ions ranging from La^{3+} to Gd^{3+}. The increase in χT is likely due to the magnetic nature and size of the lanthanide ions present. It was expected that the Mn−O−Mn ferromagnetic interactions would dominate as 3d-4f magnetic interactions are generally weak. The magnetic data shows that the paramagnetic Ln^{3+} ions in **2** (Sm) and **3** (Gd) do significantly enhance the bulk ferromagnetism compared to that of **1** (La), suggesting sizable contributions from the 4f magnetic ions.

Introduction

Exploratory synthesis of magnetic insulators containing transition metal (TM) oxide (mainly 3d) magnetic nanostructures that are structurally isolated and electronically insulated by closed-shell, diamagnetic silicate, arsenate, and phosphate oxyanions has been of great interest with respect to confined magnetic spins.[1] Studies have shown that these TM-oxide nanostructures form 0-D clusters,[2] 1-D chains,[3] and 2-D layers[4] that often imitate structural units of corresponding bulk oxides that are of technological importance. With the incorporation of lanthanides (4f) into these electronically confined transition metal (3d) oxide structures, we anticipate the formation of new magnetic nanostructures having sizable 4f contributions. The lanthanide ions provide both large spin values and considerable single-ion anisotropy. To seek new quantum magnetic solids, it therefore seems logical to extend our exploratory synthesis to heterometallic $TM-Ln^{III}$ systems.

In view of the internal nature of the 4f orbitals, lanthanide ions possess large unquenched orbital angular momentum ($L \neq 0$) with the exception of La^{3+} (f^0), Eu^{2+} (f^7), Gd^{3+} (f^7), Yb^{2+} (f^{14}), and Lu^{3+} (f^{14}). Because of the "buried" 4f electrons, crystal field effects on the lanthanide ions are small compared to that of first-row transition metal ions, and consequently, spin−orbit coupling is much larger. The latter strongly influences the magnetic properties of lanthanide containing materials. It should be noted that, although the magnetic interactions are generally weak because of the localized 4f electrons, lanthanides (with the exception of those with $L = 0$) have large single-ion anisotropy which can enhance the magnetocrystalline anisotropy in resulting solids.[5]

*To whom correspondence should be addressed. E-mail: shwu@clemson.edu.

(1) (a) Hwu, S.-J. *Chem. Mater.* **1998**, *10*, 2846–2859. (b) Queen, W. L.; Hwu, S.-J.; Wang, L. *Angew. Chem., Int. Ed.* **2007**, *46*, 5344–5347.

(2) (a) Huang, Q.; Hwu, S.-J. *Inorg. Chem.* **1998**, *37*, 5869–5874. (b) Hwu, S.-J.; Ulutagay-Kartin, M.; Clayhold, J. A.; Mackay, R.; Wardojo, T. A.; O'Connor, C. T.; Krawiec, M. *J. Am. Chem. Soc.* **2002**, *124*, 12404–12405. (c) Clayhold, J. A.; Ulutagay-Kartin, M.; Hwu, S.-J.; Koo, H.-J.; Whangbo, M.-H.; Voigt, A.; Eaiprasertsak, K. *Phys. Rev. B.* **2002**, *66*, 052403/1–052403/4. (d) Ulutagay-Kartin, M.; Hwu, S.-J.; Clayhold, J. A. *Inorg. Chem.* **2003**, *42*, 2405–2409. (e) Mo, X.; Etheredge, K.M. S.; Hwu, S.-J.; Huang, Q. *Inorg. Chem.* **2006**, *45*, 3478–3480. (f) Ranmohotti, K. G. S.; Mo, S.; Smith, M. K.; Hwu, S.-J. *Inorg. Chem.* **2006**, *45*, 3665–3670.

(3) (a) Etheredge, K. M. S.; Hwu, S.-J. *Inorg. Chem.* **1996**, *35*, 1474–1477. (b) Etheredge, K. M. S.; Hwu, S.-J. *Inorg. Chem.* **1996**, *35*, 5278–5282. (c) Ulutagay-Kartin, M.; Etheredge, K. M. S.; Shimek, G. L.; Hwu, S.-J. *J. Alloys Compd.* **2002**, *338*, 80–86.

(4) (a) Wang, S.; Hwu, S.-J. *J. Am. Chem. Soc.* **1992**, *114*, 6920–6922. (b) Wang, S.; Hwu, S.-J. *Inorg. Chem.* **1995**, *34*, 166–171. (c) Wang, S.; Hwu, S.-J.; Paradis, J. A.; Whangbo, M.-H. *J. Am. Chem. Soc.* **1995**, *117*, 5515–5522. (d) Mo, X.; Hwu, S.-J. *Inorg. Chem.* **2003**, *42*, 3978–3980.

(5) Benelli, C.; Gatteschi, D. *Chem. Rev.* **2002**, *102*, 2369–2387 and references cited therein.

Published on Web 07/29/2009

In extended solids containing mixed 3d-4f metals, there are prior examples showing that the 4f ions play a significant role in the observed physical properties. For example, in 3d-4f magnetoelectric multiferroic materials the magnetic states on the lanthanide sites are coupled to the atomic structure.[6] That is, the magnetization can be induced by the application of an electric field, or in reverse, polarization can be induced by the applications of a magnetic field.[7,8] Huge magnetoelectric effects have been observed in TM−Ln^{III} families like $LnMnO_3$ perovskite manganites[9] and hexagonal manganites,[10] where the presence of 4f ions efficiently enhance the magnetic control of polarization.[11]

In other cases, such as Ln-substituted high-T_c $YBa_2Cu_3O_{7-x}$, paramagnetic lanthanide ions do not seem to impose much of an expected effect on the superconductivity.[12] Initially, it was thought that magnetic $4f^n$ ($n > 0$) ions would decrease T_c because the interplay between magnetism and the conduction electrons were expected to destroy the Cooper pairs. Studies indicate that, because of the special atomic arrangement in the structure of triple perovskite units, the Ln^{3+} ions serve just as an electropositive cation and charge reservoir, thus the superconductivity is preserved.

Recently, work done with molecular solids pertaining to 3d-4f systems is vastly increasing, especially with respect to magnetic studies.[13] With nanomagnets such as single molecule magnets (SMMs) and single chain magnets (SCMs), the mixing of lanthanides with transition metals is based on hopes of achieving higher blocking temperatures because of the highly anisotropic nature of lanthanide ions and large S values.[14] In 3d-4f SCMs, the lanthanides' anisotropic contribution significantly compensates for the weak magnetic interactions associated with 4f ions.[15] It is our goal to synthesize extended solids that incorporate 3d-4f heterometallic, nanostructures similar to SMMs and SCMs to study structure and property correlations.

In this paper, we report the synthesis and characterization, as well as the structure and magnetic property correlations, of the $Na_3LnMn_3O_3(AsO_4)_3$ series, where Ln^{3+} = La^{3+} (**1**), Sm^{3+} (**2**), and Gd^{3+} (**3**). These compounds are isostructural where the parallel 1-D $[MnO_4]_\infty$ magnetic chains are interconnected by lanthanide cations in a 3-D lattice via oxygen. In our systematic investigation, the Ln = La^{3+} compound **1** was synthesized to acquire insight into the contribution of the paramagnetic lanthanide ions in **2** and **3**.

Experimental Section

Synthesis. Crystals of the first compound isolated in the $Na_3LnMn_3O_3(AsO_4)_3$ series, where Ln = Gd, were grown by employing a molten-salt reaction in a fused silica ampule under vacuum. Na_2O_2 (97%, Aldrich), Gd_2O_3 (99.9%, Alfa Aesar), Mn_2O_3 (99%, Aldrich), As_2O_5 (99.9%, Alfa Aesar), CsCl (99.9%, Alfa Aesar), and NaCl (99.0%, Alfa Aesar) were mixed and ground in a nitrogen-purged drybox. Approximately 0.25 g of the oxides were mixed in a 2:1:1:2 molar ratio with 0.75 g of a CsCl/NaCl (65:35 mol %) eutectic salt flux. The reaction mixture was sealed in an evacuated silica tube and then heated up to 650 at 1 °C min^{-1}, isothermed for 4 days, slowly cooled to 350 at 0.1 °C min^{-1}, and then furnace-cooled to room temperature. The crystalline phase was retrieved from the flux by washing the product with deionized water using a suction filtration method. A 40% crystalline yield of amber brown, needle crystals of **3** were isolated along with a 60% crystalline yield of brown columns of the new pseudo-low-dimensional $Na_2GdMnO(AsO_4)_2$.[16]

The $Na_3LnMn_3O_3(AsO_4)_3$ series (Ln = La^{3+}, Sm^{3+}, Gd^{3+}) can also be prepared in larger yields when a stoichiometric molar ratio, 3:1:3:3, of the corresponding reactants are used in the same CsCl/NaCl flux under the same conditions as mentioned previously.

Crystallographic Studies. Amber brown needle crystals of **1**, **2**, and **3** were physically examined and selected under an optical microscope equipped with a polarizing light attachment. The data crystals were mounted separately on glass fibers with epoxy for X-ray diffraction studies. The data were collected at room temperature on a four-circle Rigaku AFC8 diffractometer equipped with a Mercury CCD area detector, Mo Kα (λ = 0.71073 Å) radiation. The structures were solved by direct method using the SHELEX-97 program[17] and refined on F^2 by least-squares, full-matrix techniques; Table 1 reports the crystallographic data of the $Na_3LnMn_3(AsO_4)_3$ series. The compound series is isostructural; for simplicity, only atomic parameters (Table 2) of **3** are included in this report. Table 3 reports selected bond distances and angles of **1**−**3**. The structure solutions have relatively large residual peaks that are most likely due to small size and possible twinning.

Magnetic Susceptibility. Temperature-dependent magnetic measurements of **1**−**3** were carried out with a Quantum Design SQUID MPMS-5S magnetometer. The measurements were taken from 2 to 300 K in the applied field of H = 0.01 and 0.5 T. Selected crystals of **1** (5.0 mg), **2** (1.8 mg), and **3** (1.2 mg) were each ground and placed in a gel capsule sample holder. The magnetic susceptibility was corrected for the gel capsule and core diamagnetism with Pascal constants.[18] Field-dependence studies of **1** and **3** were performed at 2 and 20 K.

Results and Discussion

Crystal Structure. In Table 1, poor single crystal structure solutions obtained for compounds **1** and **2** are most likely due to small crystal size. It is noted that the stoichiometric yield syntheses for each compound have yet been successful. Powder X-ray diffraction patterns, collected on the attempted 100% yield syntheses, revealed the formation of $LnAsO_4$ at temperatures around ∼650 °C and $Na_3Ln(AsO_4)_2$ at temperatures in the range of 750−950 °C. These phases are likely a

(6) Tyson, T. A.; Chen, Z.; DeLeon, M. A.; Yoong, S.; Cheong, S.-W. *J. Magn. Magn. Mater.* **2009**, *321*, 1714–1718.
(7) Spaldin, N. A.; Fiebig, M. *Science* **2005**, *309*, 391–392.
(8) Fiebig, M. *J. Phys. D: Appl. Phys.* **2005**, *38*, R123–R152.
(9) Kimura, T.; Goto, T.; Shintani, H.; Ishizaka, K.; Arima, T.; Tokura, Y. *Nature* **2003**, *426*, 55–58.
(10) Lottermoser, T.; Lonkai, T.; Amann, U.; Hohlwein, D.; Ihringer, J.; Fiebig, M. *Nature* **2004**, *430*, 541–544.
(11) Kadomtseva, A. M.; Krotov, S. S.; Popov, Y. F.; Vorob'ev, G. P. *Low Temp. Phys.* **2006**, *32*, 709–724.
(12) (a) Tarascon, J. M.; McKinnon, W. R.; Greene, L. H.; Hull, G. W.; Vogel, E. M. *Phys. Rev. B* **1987**, *36*, 226–234. (b) Fisk, Z.; Thompson, J. D.; Zirngiebl, E.; Smith, J. L.; Cheong, S.-W. *Solid State Commun.* **1987**, *62*, 743–744. (c) Engler, E. M.; Lee, V. Y.; Nazzal, A. I.; Beyers, R. B.; Lim, G.; Grant, P. M.; Parkin, S. S. P.; Ramirez, M. L.; Vazquez, J. E.; Savoy, R. J. *J. Am. Chem. Soc.* **1987**, *109*, 2848–2849.
(13) Mishra, A.; Wernsdorfer, W.; Parsons, S.; Christou, G.; Brechin, E. K. *Chem. Commun.* **2005**, 2086–2088.
(14) Murugesu, M.; Abhudaya, M.; Wernsdorfer, W.; Abboud, K.; Christou, G. *Polyhedron* **2006**, *25*, 613–625.
(15) Bernot, K.; Bogani, L.; Caneschi, A.; Gatteschi, D.; Sessoli, R. *J. Am. Chem. Soc.* **2006**, *128*, 7947–7956.
(16) Crystallographic data for $Na_2GdMnO(AsO_4)_2$: a = 5.763(1) Å, b = 14.746(3) Å, c = 9.037(2) Å, β = 92.66(3)°, $P2_1/n$ (no. 14), Z = 4.
(17) (a) Sheldrick, G. M. In *Crystallographic Computing 3*; Sheldrick, G. M., Kruger, C., Goddard, R., Eds.; Oxford Univ. Press: London, 1985; pp 175–189. (b) Sheldrick, G. M. In *SHELXTL, Version 6.1 Structure Determination Software Programs*; Bruker Analytical X-ray Systems Inc.: Madison, WI, 2001.
(18) O'Connor, C. J. *J. Prog. Inorg. Chem.* **1982**, *29*, 203–276.

Table 1. Crystallographic Data for $Na_3LnMn_3O_3(AsO_4)_3$, Ln = La^{3+}, Sm^{3+}, Gd^{3+}

empirical formula	$Na_3LaMn_3O_3(AsO_4)_3$, **1**	$Na_3SmMn_3O_3(AsO_4)_3$, **2**	$Na_3GdMn_3O_3(AsO_4)_3$, **3**
FW	837.46	848.91	855.80
crystal system	hexagonal	hexagonal	hexagonal
crystal dimension, mm	0.10 × 0.02 × 0.02	0.05 × 0.02 × 0.02	0.4 × 0.02 × 0.02
space group, Z	$P6_3/m$ (No. 176), 2	$P6_3/m$ (No. 176), 2	$P6_3/m$ (No. 176), 2
T, °C	27	27	27
a, Å	11.167(2)	11.081(2)	11.091(2)
c, Å	6.035(1)	6.020(1)	5.954(1)
V, Å^3	651.7(2)	640.2(2)	634.3(2)
μ (Mo Kα), mm^{-1}	13.796	15.294	16.037
d_{calc}, g cm^{-3}	4.268	4.404	4.481
data/restraints/parameters	488/0/48	428/6/48	408/0/48
final R1, wR2[a] [$I > 2\sigma(I)$], GOF	0.0767/0.2021/1.214	0.0878/0.2409/1.173	0.0466/0.1318/1.101
largest diff. peak/hole, e/ Å^3	4.434/-2.441	4.538/-3.726	3.232/-1.386

[a] $R = \sum||F_o| - |F_c||/\sum|F_o|$; $wR2 = [\sum w(|F_o| - |F_c|)^2/\sum w|F_o|^2]^{1/2}$; $w = 1/[\sigma^2(F_o^2) + (0.0319\,P)^2 + 2.51P]$, where $P = (F_o^2 + 2F_c^2)/3$.

Table 2. Atomic Coordinates and Equivalent Displacement Parameters for **3**

atom	Wyckoff notation	x	y	z	U_{iso} (Å^2)[a]
Na	6*h*	0.263(1)	0.1064(8)	−1/4	0.035(2)
Gd	2*c*	1/3	2/3	1/4	0.013(1)
Mn	6*g*	1/2	1	0	0.012(1)
As	6*h*	0.5985(2)	0.8116(2)	−1/4	0.014(1)
O(1)	6*h*	0.385(1)	0.913(1)	1/4	0.013(2)
O(2)	12*i*	0.5147(9)	0.8235(8)	−0.020(2)	0.016(2)
O(3)	6*h*	0.580(1)	0.650(1)	−1/4	0.015(3)
O(4)	6*h*	0.767(1)	0.915(2)	−1/4	0.038(4)

[a] Equivalent isotropic U defined as one-third of the trace of the orthogonalized U_{ij} tensor.

Table 3. Selected Bond Distances and Angles for $Na_3LnMn_3O_3(AsO_4)_3$, Ln = La^{3+} **1**, Sm^{3+} **2**, Gd^{3+} **3**

	1	**2**	**3**
	MnO_6		
Mn−O(1)[a] × 2	1.873(8) Å	1.880(9) Å	1.882(7) Å
Mn−O(2)[a] × 2	2.116(9) Å	2.04(1) Å	2.048(7) Å
Mn−O(3)[b,c] × 2	2.01(1) Å	2.10(1) Å	2.075(8) Å
	LnO_9		
Ln−O(1)[b,d] × 3	2.54(1) Å	2.52(2) Å	2.50(1) Å
Ln−O(2)[b,d-g] × 6	2.59(1) Å	2.54(1) Å	2.482(9) Å
	AsO_4		
As−O(2)[h] × 2	1.70(1) Å	1.69(1) Å	1.696(9) Å
As−O(3)	1.69(1) Å	1.69(2) Å	1.69(1) Å
As−O(4)	1.61(2) Å	1.62(2) Å	1.64(1) Å
∠Mn[i]−O(1)−Mn	107.3(7)°	106.4(7)°	104.6(6)°
∠Mn[j]−O(3)−Mn[d]	91.0(5)°	91.7(6)°	91.7(4)°
∠Ln−O(1)−Mn[i]	106.6(5)°	106.1(6)°	106.5(4)°
∠Ln−O(2)−Mn	100.5(4)°	100.7(6)°	102.0(3)°

[a-j] Symmetry codes: (a) $-x+1, -y+2, -z$; (b) $-y+1, x-y+1, z$; (c) $y, -x+y+1, -z$; (d) $-x+y, -x+1, z$; (e) $-y+1, x-y+1, -z+1/2$; (f) $x, y, -z+1/2$; (g) $-x+y, -x+1, -z+1/2$; (h) $x, y, -z-1/2$; (i) $-x+1, -y+2, z+1/2$; (j) $x-y+1, x, z-1/2$.

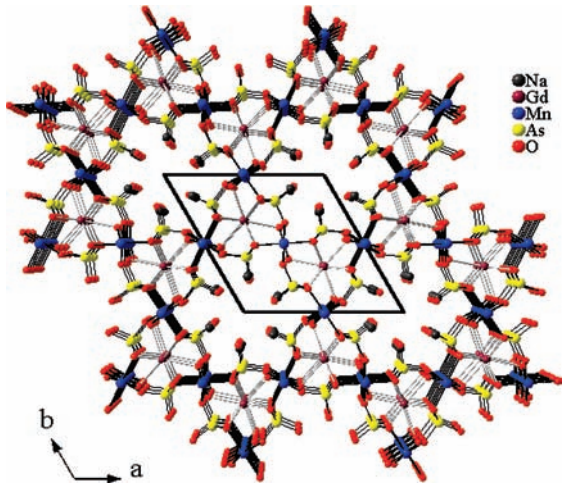

Figure 1. Perspective view along the c axis of $Na_3GdMn_3O_3(AsO_4)_3$ showing 6-fold symmetry along the 1-D channels where the Na^+ cations reside. The Gd^{3+} and As^{5+} cations connect the 1-D $[MnO_4]_\infty$ chains to form the 3-D framework. The color code of circles is the same throughout the report.

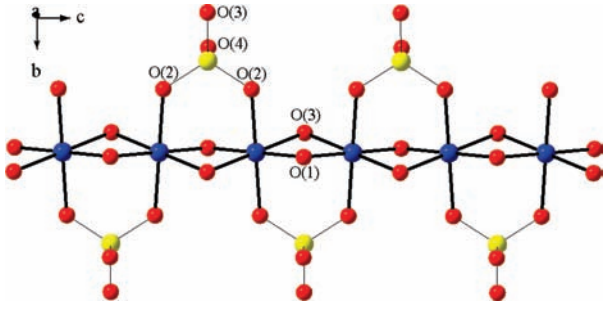

Figure 2. Partial structure of 1-D $[MnO_4]_\infty$ chain propagating along the c axis. The chain is made of fused MnO_6 units via sharing opposite edges, O(1) and O(3), and capped by As^{5+} cations. The parallel chains, not shown for clarity, are interconnected by As^{5+} cations via O(2) and O(3). O(4) is pointing toward the center of the channel where Na^+ cations reside.

thermodynamic sink which limits the formation of the targeted products.

Figure 1 presents a perspective drawing of **3** viewed along the c axis. The inversion symmetry, found at the corner of the unit cell, is surrounded by Na^+ cations inside the pseudo-one-dimensional channel. Also, there are 1-D $[MnO_4]_\infty$ chains, propagating along c, that are composed of edge-shared MnO_6 units (Figure 2). The GdO_9 polyhedra connect 3 neighboring $[MnO_4]_\infty$ chains via oxygen atoms (Figure 3). These chain units can be interconverted through a 6-fold rotation axis (parallel to c) found at the center of the 1-D channel. The GdO_9 polyhedra form tricapped trigonal prisms where each capping oxygen, O(1), is triply bridged (μ_3) with respect to $2Mn^{3+}$ and $1Gd^{3+}$. There is only one crystallographically distinct Mn^{3+} site which adopts a slightly distorted MnO_6 octahedral coordination. The parallel 1-D $[MnO_4]_\infty$ chains are linked by AsO_4 units, via O(2) and

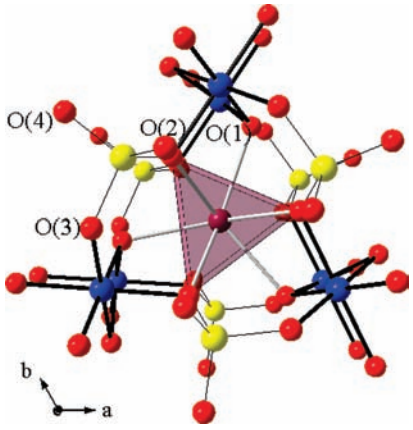

Figure 3. Gd-centered, tricapped trigonal prismatic GdO_9 polyhedral unit sharing oxygen atoms with three neighboring 1-D $[MnO_4]_\infty$ chains and six AsO_4 units, see text.

O(3) and by the trigonal prisms of the above-mentioned GdO_9 units through O(2). The apical oxygen, O(4), of the AsO_4 units point toward the empty inversion center of the channel, which appears to be the structural feature responsible for the formation of the open-framework.

Table 3 gives selected bond distances and angles corresponding to the 3d and 4f ions in the $Na_3LnMn_3O_3(AsO_4)_3$ series. The Mn(1)−O bond distances range from 1.873(8) Å to 2.116(9) Å, which are comparable to the sum of the Shannon crystal radii for a high-spin, 6-coordinate Mn^{3+} and O^{2-}, 1.995 Å.[19] The observed Ln−O distances in **1**−**3** (Table 3) are in close comparison with the calculated Shannon crystal radii for 9-coordinate Ln^{3+} and O^{2-}: 2.566 Å for La^{3+}, 2.482 Å for Sm^{3+}, and 2.457 Å for Gd^{3+}, respectively. Because of the difference in the coordination environment of O(1) and O(3), there are two ∠Mn−O(1,3)−Mn bond angles within the edge-shared chain. Since 3d-3d magnetic interactions are relatively strong compared to 3d-4f interactions, it is important to pay attention to the∠Mn−O−Mn bond angles. Compound **1** (Ln = La) shows the highest and lowest ∠Mn−O−Mn angle compared to **2** and **3**. Notice that O(1) is the μ_3 oxygen shared by 2Mn and 1Ln centers, and the angle containing O(1) gets smaller upon substituting smaller lanthanide ions. The other angle, containing O(3), is smallest when the lanthanide is largest. The distances between the Ln−Mn and Mn−Mn centers are as follows: d_{La-Mn} is 3.5592(4) Å and d_{Mn-Mn} is 3.0173(6) Å for compound **1**, d_{Sm-Mn} 3.5353(4) Å and d_{Mn-Mn} 3.0099(6) Å for **2**, d_{Gd-Mn} 3.5307(4) Å and d_{Mn-Mn} 2.9770(6) Å for **3**. These distances show that the smaller the Ln^{3+} ion, the shorter the Mn−Mn distance; this is consistent with the sum of ∠Mn−O−Mn bond angles observed for compound **3** (Ln = Gd), which is the smallest of the 3 derivatives. It is also evident in Table 3 that the Ln−O(1) capping distance does not show a significant change throughout the series; however, the Ln−O(2) distance and the size of the trigonal prism appear to follow the trend of the lanthanide contraction.

Magnetic Properties. Approaches for studying the magnetic interactions of these 3d-4f structures were conceptually based on efforts employed for molecular materials;[5] some experimental procedures and fundamental reasons are highlighted in the proceeding paragraphs. Notably, the work of Kahn et al. in which the isostructural series of the solvated ladder-type $\{Ln_2[M(opba)]_3\}$ ($\equiv Ln_2M_3$) structures was synthesized for most of the lanthanides and M equal to Cu^{2+} or Zn^{2+}.[20] Because Zn^{2+} is diamagnetic and the 3d ions are isolated from one another, when subtracting the magnetic response of Ln_2Zn_3 from that of Ln_2Cu_3, the nature of the 3d-4f magnetic interactions (nearest neighbor) reportedly can be seen by deviations from the Curie law at low temperatures. Next nearest neighbor interactions (3d-3d interactions) were found to be weak as evidenced by the magnetic studies of the Ln = La derivatives.

Furthermore, a simple mechanism for 3d-4f magnetic interactions was proposed by Kahn et al. based on a charge transfer in which coupling between Gd^{3+} and Cu^{2+} is attributed to an admixed ground state and charge transfer excited state.[21] An electron from a singly occupied 3d orbital of Cu^{2+} is transferred to an empty 5d orbital of Gd^{3+}. On the basis of Hund's rule, spin is maintained to give a maximum S resulting in a ferromagnetic interaction between Gd−Cu. The mechanism suggested that the spin states between 3d and 4f are always ferromagnetic; however, with lanthanides containing less than a half-filled f shell, the spin and orbital momentum couple antiparallel ($L - S$) leading to an overall antiferromagnetic (AFM) interaction between 3d and 4f ions. With lanthanides containing more than a half-filled f shell, the spin and orbital momentum are paired parallel ($L + S$) leading to an overall ferromagnetic (FM) interaction.[22]

On the basis of our temperature-dependent magnetic studies of **1**−**3**, it was determined that all three compounds exhibit a positive deviation from that of an ideal paramagnet which suggests ferromagnetic ordering (Supporting Information, Figure S1). Figure 4 shows a χT versus T plot for each compound. Compounds **1** and **2** show ordering temperatures (T_C) around ∼20 K; whereas, compound **3** shows an increased ordering temperature around ∼30 K, suggesting stronger ferromagnetic coupling. The magnetic data for compound **1**, the Ln = La^{3+} ($S = 0$, $L = 0$) derivative, gives us a reasonable idea of the 4f magnetic contributions because this magnetic data is that solely of Mn−O−Mn ferromagnetic interactions (primarily between nearest neighbor Mn). Although the nature of the interaction involving the spin−orbit of Sm^{3+} to the spin of Mn^{3+} is unknown, there is a more positive contribution in the χT signal at low temperatures relative to that of compound **1**. This suggests that the 3d-4f interaction of **2** can be denoted as $S_{Mn} + (L_{Sm} - S_{Sm})$, where $S = 5/2$ and $L = 5$ for Sm^{3+}. This means that the orbital contribution from the Sm^{3+} ion, which is greater than the AFM spin contribution, S_{Sm}, couples ferromagnetically to the spin of Mn^{3+} giving rise to an increase in the low temperature χT signal relative to **1**. On the reverse side, if the spins between

(19) Shannon, R. D. *Acta Crystallogr.* **1976**, *A32*, 751–767.

(20) Kahn, M. L.; Mathonière, C.; Kahn, O. *Inorg. Chem.* **1999**, *38*, 3692–3697.

(21) Andruh, M.; Ramade, I.; Codjovi, E.; Guillou, O.; Kahn, O.; Trombe, J. C. *J. Am. Chem. Soc.* **1993**, *115*, 1822–1829.

(22) Kahn, O.; Guilliou, O. In *New Frontiers in Magnetochemistry*; O'Conner, C J., Ed.; World Scientific: Singapore, 1993.

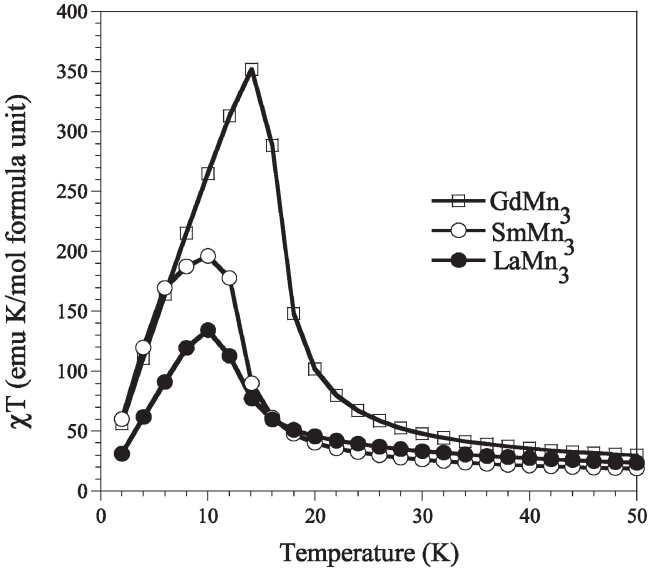

Figure 4. Field induced (0.01 T) low temperature χT vs T plots of **3** ($GdMn_3$), **2** ($SmMn_3$), and **1** ($LaMn_3$) all showing positive deviation from paramagnetic behavior. The T_C for **1** and **2** is ~20 K and that for **3** is ~30 K.

Mn^{3+} and Sm^{3+} were FM, $S_{Mn} - (L_{Sm} - S_{Sm})$, the low temperature χT signal would be less for **2** than observed for **1** because L is greater than S. The low temperature χT signal for **3** is the largest which suggests that the total value of S (7/2 for Gd^{3+}) plays a significant role in enhancing the χT signal when the Gd−O−Mn interaction is ferromagnetic. Given $L = 0$ for Gd^{3+}, this increased χT signal for **3** also suggests that the spins of Gd^{3+} and Mn^{3+} are FM which is contrary to the AFM coupled spin observed for Sm^{3+} and Mn^{3+} in **2**. The latter is more than likely the effect of the unquenched orbital contribution present in Sm^{3+}. Attempts to substitute Sm^{3+} ($^6H_{5/2}$) with Dy^{3+} ($^6H_{15/2}$) for a comparative study were so far unsuccessful.

Structurally, ferromagnetic interactions between the Mn^{3+} centers are possible as a result of the edge-sharing $Mn^{3+}O_6$ polyhedra. A possible ferromagnetic exchange could be explained based on orthogonality when paramagnetic centers are bound 90° to each other through a bridging ligand, such as O^{2-}. In other words, when the corresponding orbitals of the bridging ligands are completely orthogonal, there is no overlap for the traditional antiferromagnetic super-exchange; a ferromagnetic potential exchange is likely.[23] We are unable to confirm whether or not the enhanced χT signal at low temperatures is due to the 4f contributions or due to the magnetic interactions between the Mn^{3+} centers as a result of small structural changes from substituting the various lanthanides in **1**−**3**. It is possible that the increased χT signal is a combination of both previously mentioned cases. Since structural changes like the Mn−O−Mn bond angles are within the standard deviation of one another, it appears that the low-temperature χT deviation is largely in part due to the magnetic contributions of the lanthanide ions for **2** and **3**.

From ~100−300K, compounds **1**−**3** obey ideal Curie−Weiss behavior with visible deviations below 50 K, see Supporting Information, Figure S1a−c. The least-squares fit of the molar magnetic susceptibility data at high temperature (120−300 K, the linear portion of the curve) to the Curie−Weiss equation, $\chi = C/(T - \theta)$, where C is the Curie constant, θ is the Weiss constant, and T is the temperature, yielded the best-fit values of $C = 14.677(3)$ emu K mol^{-1}, and $\theta = 38.5(5)$ K for **3**. The calculated μ_{eff} of 10.9(1) μ_B is slightly smaller than the ideal value of 11.6 μ_B, a spin-only value for $3Mn^{3+}$ and $1Gd^{3+}$ paramagnetic ions. A positive Weiss constant suggests a ferromagnetic interaction between nearest neighbors at high temperature. To acquire a comparison, the fit for compound **1** yielded the best-fit values of $C = 7.768(3)$ emu K mol^{-1}, and $\theta = 52.7(4)$ K. The calculated μ_{eff} of 7.9(1) μ_B is consistently smaller than the ideal value of 8.5 μ_B, a spin-only value for $3Mn^{3+}$ paramagnetic ions. The fit for compound **2** yielded the best-fit values of $C = 6.268(4)$ emu K mol^{-1}, and $\theta = 54.4(8)$ K. The calculated μ_{eff} of 7.1(2) μ_B is a good deal smaller than the ideal value of 8.5 μ_B, a spin-only value for $3Mn^{3+}$ and a spin−orbit value for $1Sm^{3+}$ paramagnetic ions. Notice that the magnetic moment considering the spin−orbit contribution is relatively negligible (0.85 μ_B) for a Sm^{3+} ion (Supporting Information, Table S1).[24]

The theoretical versus experimental calculations of the magnetic moment for **1** and **3** have similar deviations from the ideal values. Because the deviations are similar in **1** and **3** it is expected that their difference is related to the Mn^{3+} ions. The more significant deviation for **2** can be attributed to the additional contributions from the low-lying excited state of Sm^{3+} ($^6H_{7/2}$); in this state there is more $(L + S)$ character, less $(L - S)$ character and $S > L$ relative to the $^6H_{5/2}$ ground configuration. Admixing of this $^6H_{7/2}$ state at higher temperatures could result in deviations solely associated with the single Sm^{3+} ion in the sense that at higher temperatures spin becomes more dominant (because of this admixing) which leads to a reduction in the overall magnetic moment. As a result of Sm^{3+} having an admixing of low-lying J multiplets, it is possible that J is no longer a fixed quantum number in other words L and S may have different temperature dependencies. Geller et al. ascribe the temperature dependencies of L and S for Sm^{3+} to explain the reduction of the magnetic moment seen at higher temperatures for Samarium Iron Garnet (SmIG).[25] Upon increasing temperatures L_{Sm} decreases faster than S_{Sm} which implies that spin is more dominant at higher temperatures; this results in a subtraction of magnetic moments of the Sm^{3+} contribution from that of the iron sublattices. On the basis of our suggestive case for the low-temperature magnetic behavior of **2** where $S_{Mn} + (L_{Sm} - S_{Sm})$, we would expect to see a decrease in the magnetic moment when $S_{Sm} > L_{Sm}$ which would occur at higher temperatures, and in fact, we do see this decrease based on our observed magnetic moment.

The field-dependent magnetic studies below T_c show what is representative of soft ferromagnetism for all three compounds. Figure 5 shows the 2 and 20 K field

(23) Curély, J. *Monatsh. Chem.* **2005**, *136*, 1013–1036 and references cited therein.

(24) $g = 3/2 + [S(S+1) - L(L+1)]/2J(J+1)$; $g = 2/7$ for Sm^{3+} where $S = 5/2$, $L = 5$, $J = 5/2$; $\mu = g[J(J+1)]^{1/2} = 0.85\,\mu_B$.

(25) Geller, S.; Williams, H. J.; Sherwood, R. C.; Remeika, J. P.; Espinosa, G. P. *Phys. Rev.* **1963**, *131*, 1080–1082.

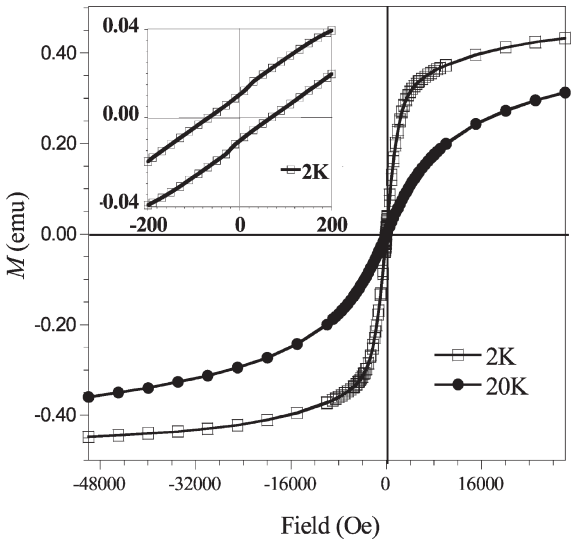

Figure 5. Field-dependent hysteresis of **3** at 2 and 20 K. The inset shows very small coercive field and remnant magnetization at 2 K.

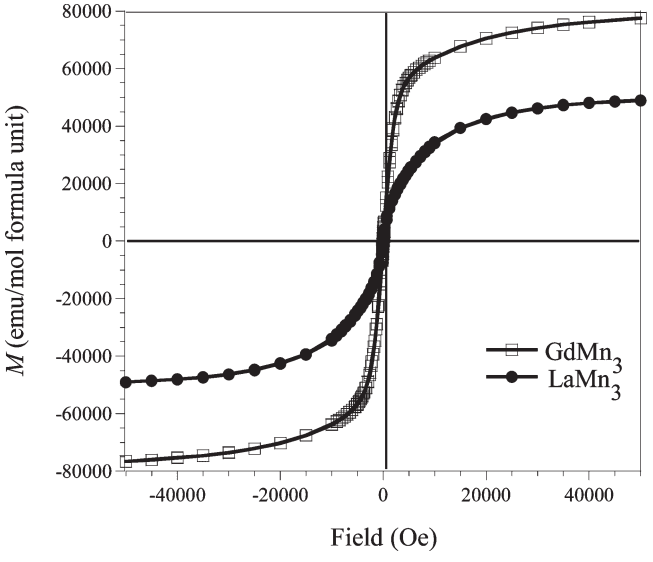

Figure 6. Field-dependence sweep of **1** and **3** at 2 K showing additional magnetization with use of paramagnetic lanthanide ion (Gd^{3+}) over that of diamagnetic lanthanide ion (La^{3+}).

dependence of **3**. The inset shows a small coercive field (~70 Oe). It is observed that, as shown in Figures 6 and Supporting Information, Figure S2, there is an additional magnetization as would be expected when replacing La^{3+} with Gd^{3+} if the interaction between Gd^{3+} and Mn^{3+} is ferromagnetic. Although field-dependence measurements of **2** have not yet been performed, the curve for **2** is expected to lie between the curves of **1** and **3**. Data points extracted from the 2 K magnetic susceptibility measurements of **2** at 100 and 5000 Oe confirm that this is indeed the case.

Final Remarks. A newly discovered series of $TM-Ln^{III}$ arsenates, $Na_3LnMn_3O_3(AsO_4)_3$, provides an opportunity for the systematic study of magnetic contributions from otherwise "buried" electrons in f obitals. This isostructural series exhibits magnetic nanostructures of $[MnO_4]_\infty$ magnetic chains interconnected by Ln^{3+} cations. The structure and magnetic property correlations suggest that the increased magnetic response relative to the La phase could be attributed to the combination of 4f magnetic contributions and tiny structural changes that alter the Mn−O−Mn interactions in the 1-D $[MnO_4]_\infty$ chain. One would expect the Mn−O−Mn interaction to be the dominant contribution to the bulk ferromagnetic properties. The Weiss constants consistently suggest that nearest neighbor interactions (Mn−O−Mn) are ferromagnetic at high temperatures. A true measurement of the lanthanide's magnetic contribution may come to light if we could substitute a diamagnetic ion, such as Ga^{3+}, for Mn^{3+} in the $Na_3LnMn_3O_3(AsO_4)_3$ series. Likewise, there is a need for magnetic data of 3d-4f materials to gain insight that will further the understanding of 3d-4f magnetic interactions; especially when the 4f ion has orbital contribution. Work is in progress to study the $Na_3LnMn_3O_3(AsO_4)_3$ series in greater detail, specifically for the f^n cases where $n > 7$. Orientation-dependent magnetic studies are also going to be investigated. The magnetochemistry of diluted, low-dimensional, 3d-4f extended solids is not well established because of the lack of compounds of this type. Comparatively speaking, it will be interesting to study the magnetic properties of the $Na_2GdMnO(AsO_4)_2$ phase which also features 1-D $[MnO_4]_\infty$ chains with alternating GdO_8 units.[16] Not only are the paramagnetic ions further separated by AsO_4 units in this new phase, but the Gd/Mn ratio is larger than that of the title series. A systematic approach in the investigation of magnetic properties is currently underway, and comparisons will be reported later in a separate article.

Acknowledgment. Financial support for this research (DMR-0322905, 0706426) and the purchase of a single crystal X-ray diffractometer (CHE-9808165) and SQUID magnetometer (CHE-9808044) from the National Science Foundation (NSF) is gratefully acknowledged.

Supporting Information Available: X-ray crystallographic file (in CIF format) and temperature-dependent magnetic susceptibility data of **1**−**3**. This material is available free of charge via the Internet at http://pubs.acs.org.